IEEE Access
Multidisciplinary ⋮ Rapid Review ⋮ Open Access Journal

Received July 10, 2020, accepted July 27, 2020, date of publication July 29, 2020, date of current version August 11, 2020.

Digital Object Identifier 10.1109/ACCESS.2020.3012709

Inherently Non-Pulsating Input Current DC-DC Converter for Battery Storage Systems

GUIDONG ZHANG[1], (Member, IEEE), NA JIN[1], LILI QU[2], AND SAMSON SHENGLONG YU[3], (Member, IEEE)

[1]School of Automation, Guangdong University of Technology, Guangzhou 510006, China
[2]School of Automation, Foshan University, Foshan 528225, China
[3]School of Engineering, Deakin University, Melbourne, VIC 3216, Australia

Corresponding author: Lili Qu (qulili@fosu.edu.cn)

This work was supported in part by the National Natural Science Foundation of China under Grant 51907032 and Grant 61733015; in part by the Natural Science Foundation of Guangdong Province under Grant 2018A030313365; and in part by the Science and Technology Planning Project of Guangzhou under Grant 201804010310.

ABSTRACT With an ever-growing number of batteries being integrated into the electric grid, bidirectional converters with non-pulsating dc input current are required to replace the existing bidirectional converters so as to extend the lifetime of such dc power suppliers. Bidirectional DC-DC converters are increasingly used in a variety of applications including uninterruptable power supplies, electric vehicles and renewable energy systems. In this study, we propose a new topology of bidirectional dc-dc converter with inherently non-pulsating input current (NPIC), which is intended to be used for battery energy storage systems. With simple modifications from the conventional converters, the proposed NPIC converter has no inherent pulsating input current in the step-down (buck) mode under both continuous and boundary conduction modes (CCM and BCM), whereas in the step-up (boost) mode, the proposed NPIC converter retains the desired voltage gain. Underpinning theories, operating principles and steady-state performances are analyzed and presented in detail, which are then corroborated by simulation and experimentation. The proposed converter topology, with simple design principle and ease for implementation, is likely to have wide-ranging applicability in interfacing electrochemically functioned dc sources to modern power systems.

INDEX TERMS Bidirectional dc-dc converter, non-pulsating input current, step-up mode, step-down mode, continuous conduction mode, boundary conduction mode.

I. INTRODUCTION

In renewable energy integrated hybrid power systems, hybrid vehicle energy systems and uninterruptible power supply systems, multiple dc power sources need to transfer energy to other dc energy storage systems, which requires bi-directional dc-dc converters [1]–[4]. The topology of bidirectional dc-dc converter can be divided into isolated (transformer-integrated) and non-isolated (without transformer) types. Flyback converters, forward-flyback converters, half-bridge converters and full-bridge converters are typical bidirectional isolated dc-dc converters [5]–[7]. By adjusting the turns ratio of the transformer, this converter family can obtain large voltage gains in both step-up and step-down modes. However, the power leakage generated by the converter cannot be recovered, causing a low efficiency. Compared to isolated bidirectional dc-dc converter, non-isolated converters have smaller volume and higher efficiency due to the absence of transformer [8]–[10]. Conventional buck/boost converters are widely used due to their simple topologies and required control strategies, but these converters cannot operate in extensively wide voltage-conversion range [11], [12]. For zeta/sepic and cuk/cuk type converters, energy transfer efficiency is low because of their two-stage structures [13]–[15]. In order to improve the efficiency and increase the voltage-conversion range, many new non-isolated bidirectional dc-dc converters have been proposed. Authors in [16] proposed a non-isolated bidirectional dc-dc converter with high voltage gain comprised of two boost converters; authors in [17] and [18] proposed two non-isolated bidirectional dc–dc converter topologies, with a simple circuit structure. Their

The associate editor coordinating the review of this manuscript and approving it for publication was Zhilei Yao.

experimentally proven superior voltage step-up performances have extended their applicability to wide-ranging voltage levels than conventional converters.

However, the above-mentioned converters only consider voltage gain and device stress, without taking into account the impact of dc pulsating input current on the input power supply. For example, the buck/boost bidirectional converter operating in step-down mode is equivalent to a buck converter, and input current of the converter is equal to the inductor current when the switch is turned on and becomes zero when the switch is turned off, causing the converter to have a pulsating input current [19]. The pulsating input current of these bidirectional converters may degrade the performance and lifespan of the electrochemically functioned power sources or energy storage systems, because the pulsating current can lead to an accelerated aging rate of the electrodes [20]–[22], which may also cause problems like electromagnetic interference, slow transient response, and reduction of energy efficiency.

It is well known that large electrolytic capacitors connected to the input port can cope with the inherent pulsating input current issue, however, this solution is executed at the expense of deterioration of the electrolytic capacitor, which can shorten the lifespan of the overall converter system [22], [23]. Another feasible option may be replacing the bulky electrolytic capacitor with an *LC* filter, which, however, may degrade energy efficiency and affect the dynamic performance of the converter [24], [25]. Interleaved converter could be another reasonable solution to alleviate the pulsating input current issue, but this method has been proven to be not suitable for bidirectional dc–dc converters [26], [27].

Knowing the need of non-pulsating input current converters and the shortage of a proper design, in this study, we propose a novel bidirectional dc-dc converter, which, compared to its conventional counterparts, is able to draw NPIC from the dc source while operating in the buck mode. At the same time, the proposed NPIC bidirectional converter is also able to retain its high voltage gain when working in the boost mode. Simulation and experimentation are conducted in this study, which verify the functionality and effectiveness and the proposed converter structure. The proposed NPIC converter has a simple topological design, and is easy to implement and apply to industrial uses.

The remainder of the paper is organized as follows. The structure and operating principle in buck and boost modes are detailed in Section II. Simulations and experiments are conducted with their results shown in Section III and Section IV respectively. Finally, a conclusion is drawn in Section V.

II. OPERATING PRINCIPLE OF THE PROPOSED NPIC CONVERTER

Fig. 1 shows the configuration of the proposed converter, which mainly consists of two inductors L_1 and L_2, one capacitor C_b, two switches S_1 and S_2. Steady-state analysis of the proposed converter in step-up and step-down modes is discussed as follows. It is worth-noting that inductor L_1 is

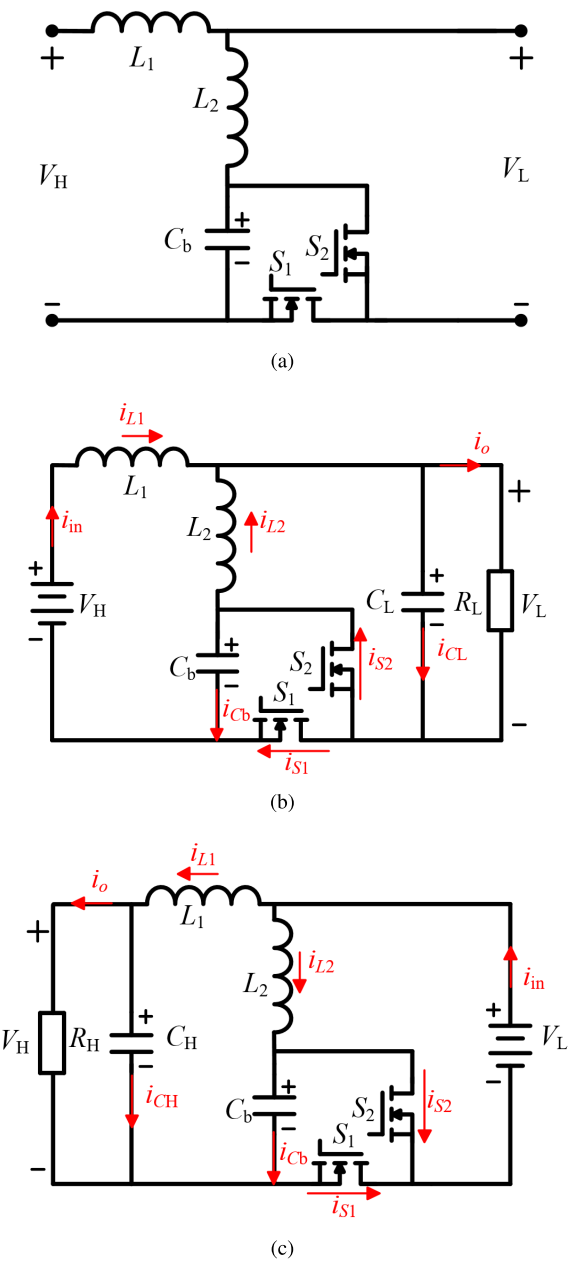

FIGURE 1. (a) Proposed converter. (b) Equivalent circuit in the step-down mode. (c) Equivalent circuit in the step-up mode.

connected in series with the input source, with contributes to the NPIC feature of the proposed converter. In order to simplify the analysis, some reasonable assumptions are made as: a) all semi-conductor devices and passive components are considered ideal; b) capacities of the capacitors are large enough to keep the capacitor voltages nearly constant.

A. STEP-DOWN MODE OF THE PROPOSED NPIC CONVERTER

The proposed converter in step-down mode is shown in Fig. 1(b). Characteristic waveforms of the proposed converter in CCM are depicted in Fig. 3, and the current flow path in one switching period is illustrated in Fig. 2(a).

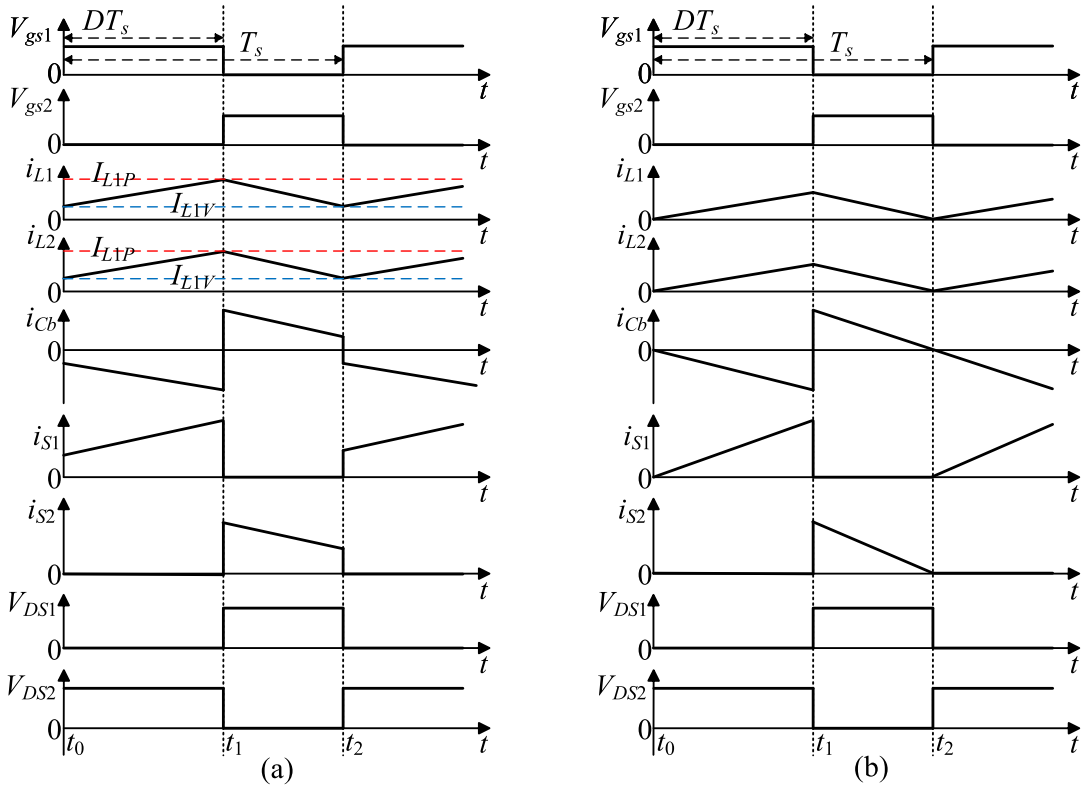

FIGURE 2. Key waveforms of the proposed converter in the step-down mode: (a) CCM; (b) BCM.

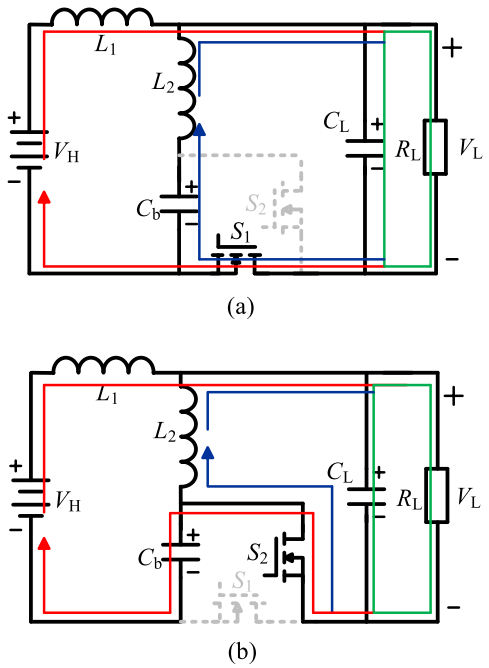

FIGURE 3. Equivalent circuits in step-down mode: (a) mode 1; (b) mode 2.

1) OPERATION MODES

Mode 1 [$t_0 < t < t_1$]: As shown in Fig. 3 (a), switch S_1 is turned on at $t = t_0$ and switch S_2 is turned off. The input source delivers energy to inductor L_1 and the load. Therefore, inductor L_1 starts to store energy, and accordingly the current flowing through inductor L_1 (i_{L_1}) increases. At the same time, energy saved in capacitor C_b is released to inductor L_2 and the load. Correspondingly, the current of inductor L_2 (i_{L_2}) starts increasing. In addition, current and voltage stresses of switches S_1 and S_2 in this mode can be found in Fig. 2 (a). Accordingly, the following equations among the components during this time interval can be obtained,

$$\begin{cases} i_{L_1}(t) = I_{L1V} + \dfrac{v_{\mathrm{H}} - v_{\mathrm{L}}}{L_1} t, \\ i_{L_2}(t) = I_{L2V} + \dfrac{v_{\mathrm{Cb}} - v_{\mathrm{L}}}{L_2} t, \\ i_{C_b}(t) = -I_{L2V} - \dfrac{v_{\mathrm{Cb}} - v_{\mathrm{L}}}{L_2} t, \\ i_{C_{\mathrm{L}}}(t) = I_{L1V} + I_{L2V} + (\dfrac{v_{\mathrm{H}} - v_{\mathrm{L}}}{L_1} + \dfrac{v_{\mathrm{Cb}} - v_{\mathrm{L}}}{L_2})t - i_{\mathrm{o}}, \end{cases} \tag{1}$$

where v_{H} is the input voltage, v_{Cb} is the voltage of the capacitor C_b, v_{L} is the output voltage and I_{L1V} and I_{L2V} are the minimum values of the currents flowing through inductors L_1 and L_2, respectively.

Mode 2 [$t_1 < t < t_2$]: In this mode, S_1 is turned off and S_2 is turned on at $t = t_1$ as shown in Fig. 3 (b). During this mode, energy stored in L_1 and the input power source is delivered to the load and C_b. Hence, the current flowing through L_1 decreases. Meanwhile, inductor L_2 releases energy to the load and the current flowing through it keeps decreasing as

depicted in Fig. 2 (a). Main equations among the components during this time interval can be deduced as,

$$\begin{cases} i_{L_1}(t) = I_{L1P} - \dfrac{v_{\rm H} - v_{C\rm b} - v_{\rm L}}{L_1}t, \\ i_{L_2}(t) = I_{L2P} - \dfrac{v_{\rm L}}{L_2}t, \\ i_{C_{\rm b}}(t) = I_{L1P} - \dfrac{v_{\rm H} - v_{C\rm b} - v_{\rm L}}{L_1}t, \\ i_{C_{\rm L}}(t) = I_{L1P} + I_{L2P} - (\dfrac{v_{\rm H} - v_{C\rm b} - v_{\rm L}}{L_1} + \dfrac{v_{\rm L}}{L_2})t - i_{\rm o}, \end{cases} \tag{2}$$

where I_{L1P} and I_{L2P} are the maximum values of the currents flowing through the inductors L_1 and L_2, respectively.

Assuming the converter is a lossless system and the voltage ripples are ignorable in a switching period. Based on the mode analysis and applying volt-second balance principle to inductors L_1 and L_2, steady-state voltage relationships among input voltage, output voltage, and capacitor voltages can be obtained as,

$$\begin{cases} (V_{\rm H} - V_{\rm L})D + (V_{\rm H} - V_{C\rm b} - V_{\rm L})(1 - D) = 0, \\ (V_{C\rm b} - V_{\rm L})D - V_{\rm L}(1 - D) = 0, \end{cases} \tag{3}$$

where D is the duty cycle of switch S_1.

From (3), the voltage of capacitor $C_{\rm b}$ and voltage of capacitor $C_{\rm L}$, i.e., the output voltage, can be derived as,

$$\begin{cases} V_{C\rm b} = V_{\rm H}, \\ V_{\rm L} = DV_{\rm H}. \end{cases} \tag{4}$$

According to (4), the voltage conversion ratio of the proposed converter can be expressed as,

$$G_{step-down} = \frac{V_{\rm L}}{V_{\rm H}} = D. \tag{5}$$

2) INDUCTOR CURRENTS

Applying the ampere-second balance theorem for the capacitor current, we can have

$$\int_0^{T_{\rm s}} i_C(t)dt = 0, \tag{6}$$

where $T_{\rm s}$ is the switching period.

Considering (1), (2), (4) and (6), the maximum and minimum values of the inductor currents can be calculated as,

$$I_{L1P} = DI_{\rm o} + \frac{V_{\rm H} - V_{\rm L}}{2L_1}DT_{\rm s}, \tag{7}$$

$$I_{L1V} = DI_{\rm o} - \frac{V_{\rm H} - V_{\rm L}}{2L_1}DT_{\rm s}, \tag{8}$$

$$I_{L2P} = (1 - D)I_{\rm o} + \frac{V_{\rm H} - V_{\rm L}}{2L_2}DT_{\rm s}, \tag{9}$$

$$I_{L2V} = (1 - D)I_{\rm o} - \frac{V_{\rm H} - V_{\rm L}}{2L_2}DT_{\rm s}, \tag{10}$$

where $I_{\rm o}$ is the load current. The average current of each inductor can be derived as,

$$\bar{I}_{L1} = DI_{\rm o}, \tag{11}$$

$$\bar{I}_{L2} = (1 - D)I_{\rm o}. \tag{12}$$

Then, current ripples of the inductors can be deduced as,

$$\Delta i_{L_1} = \frac{V_{\rm H} - V_{\rm L}}{L_1}DT_{\rm s}, \tag{13}$$

$$\Delta i_{L_2} = \frac{V_{\rm H} - V_{\rm L}}{L_2}DT_{\rm s}. \tag{14}$$

3) VOLTAGE AND CURRENT STRESSES OF POWER DEVICES

According to the above analysis, it can be obtained that the voltage stresses of switches S_1 and S_2 in the proposed converter, namely, V_{S_1} and V_{S_2}, are equal to the voltage of the capacitor $C_{\rm b}$, i.e., $V_{C_{\rm b}}$, as shown in (4).

According to Fig. 2(a), peak currents flowing through switches S_1 and S_2 can be derived as,

$$I_{\rm peak}^{S_1} = I_{L1P} + I_{L2P}, \tag{15}$$

$$I_{\rm peak}^{S_2} = I_{L1P} + I_{L2P}. \tag{16}$$

By applying (5), (7), and (9) to (15) and (16), equations (15) and (16) can be rewritten as follows,

$$I_{\rm peak}^{S_1} = I_{\rm peak}^{S_2} = I_{\rm o} + \frac{V_{\rm L}(V_{\rm H} - V_{\rm L})}{2L_e f_{\rm s} V_{\rm H}}, \tag{17}$$

where $L_e = L_1//L_2$.

4) CRITICAL INDUCTANCE L_{1c} AND L_{2c}

When $I_{L1V} = 0$, the critical inductance of the inductor L_1 can be derived as,

$$L_{1c} = \frac{R_{\rm L}(1 - D)T_{\rm s}}{2D}, \tag{18}$$

where $R_{\rm L} = V_L/I_{\rm o}$. Incorporating (4), (18) can be rewritten as,

$$L_{1c} = \frac{R_{\rm L}(V_{\rm H} - V_{\rm L})}{2V_{\rm L}f_{\rm s}}. \tag{19}$$

Similarly, the critical inductance of inductor L_2 can be derived as,

$$L_{2c} = \frac{V_{\rm L}R_{\rm L}}{2V_{\rm H}f_{\rm s}}. \tag{20}$$

When inductances L_1 and L_2 are equal to critical values, the converter operates in the boundary-conduction-mode (BCM) mode. Fig. 2 (b) shows some typical waveforms in BCM operation.

5) OUTPUT VOLTAGE RIPPLE ANALYSIS IN CCM

According to the characteristics of the capacitor, voltage ripples of the capacitor can be calculated as,

$$v_C^{rip} = \frac{1}{C}\int_{t_{01}}^{t_{02}} i_C(t)dt, \tag{21}$$

where t_{01} is the time that the current flowing through it changes from positive to negative, and t_{02} is the time that the current flowing through the capacitor changes from negative to positive.

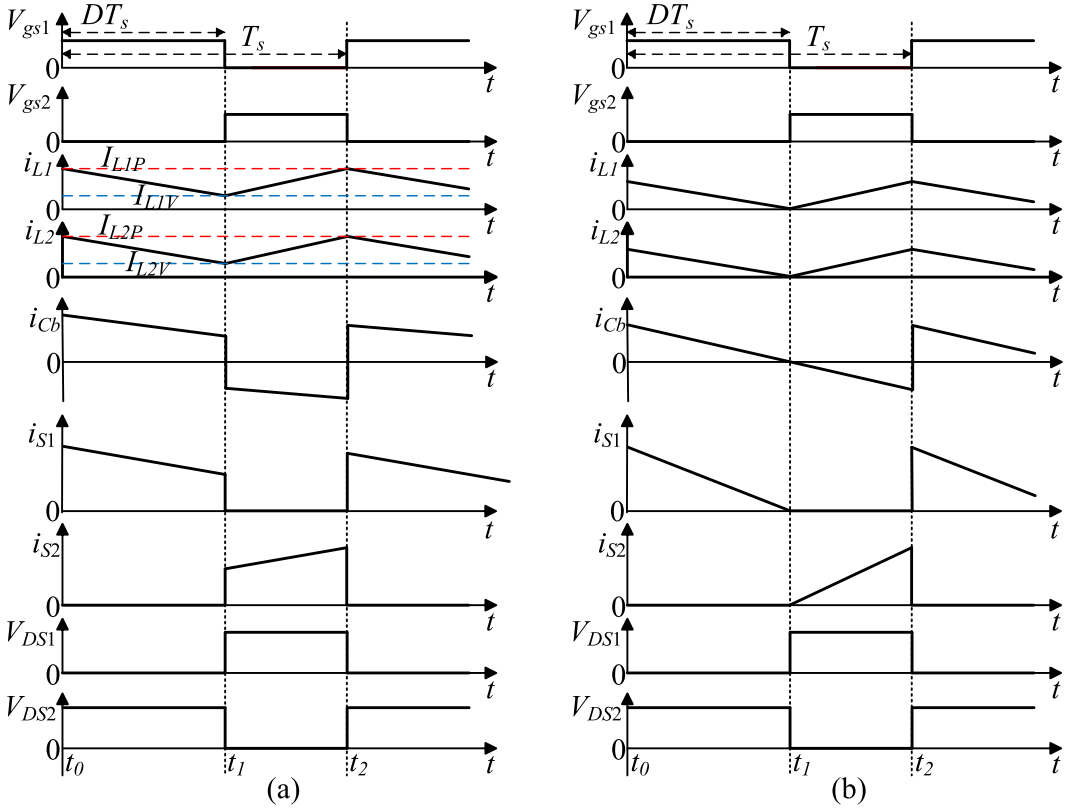

FIGURE 4. Key waveforms of the proposed converter in the step-up mode: (a) CCM.; (b) BCM.

For capacitor C_{L}, the voltage ripple can be calculated as,

$$v_{\mathrm{CL-rip}}^{CCM} = \frac{1}{C_{\mathrm{L}}}\int_{t_{01}}^{t_{02}} i_{C_{\mathrm{L}}}(t)dt, \tag{22}$$

where t_{01} and t_{02} can be calculated as,

$$t_{01} = \frac{L_{\mathrm{e}}(I_{\mathrm{o}} - I_{L1V} - I_{L2V})}{V_{\mathrm{H}} - V_{\mathrm{L}}} = \frac{DT_{\mathrm{s}}}{2}, \tag{23}$$

$$t_{02} = \frac{L_{\mathrm{e}}(I_{\mathrm{o}} - I_{L1P} - I_{L2P})}{V_{\mathrm{L}}} = -\frac{(1-D)T_{\mathrm{s}}}{2}. \tag{24}$$

From (21)–(24), the voltage ripple can be calculated as,

$$v_{\mathrm{CL-rip}}^{CCM} = \frac{V_{\mathrm{L}}(V_{\mathrm{H}} - V_{\mathrm{L}})}{8L_{\mathrm{e}}C_{\mathrm{L}}V_{\mathrm{H}}f_{\mathrm{s}}^2}. \tag{25}$$

B. STEP-UP MODE OF THE PROPOSED CONVERTER

The proposed converter in step-up mode is shown in Fig. 1(c), whose equivalent circuits in CCM mode are depicted in Fig. 5, and the characteristic waveforms are illustrated in Fig. 4(a).

1) OPERATION MODES

Mode 1 [$t_0 < t < t_1$]: As shown in Fig. 5 (a), S_1 is turned on and S_2 is turned off. Input source V_{L} and L_1 and L1 supply power to the load, so i_{L_1} decreases. At the same time, L_2 and C_{b} release energy to the load, so i_{L_2} and $i_{C_{\mathrm{b}}}$ also decrease. Therefore, the following equation set relating the electric quantities of the components during this time interval can be obtained,

$$\begin{cases} i_{L_1}(t) = I_{L1P} - \dfrac{v_{\mathrm{H}} - v_{\mathrm{L}}}{L_1}t, \\ i_{L_2}(t) = I_{L2P} - \dfrac{v_{\mathrm{Cb}} - v_{\mathrm{L}}}{L_2}t, \\ i_{C_{\mathrm{b}}}(t) = I_{L2P} - \dfrac{v_{\mathrm{Cb}} - v_{\mathrm{L}}}{L_2}t, \\ i_{C_{\mathrm{L}}}(t) = I_{L1P} - \dfrac{v_{\mathrm{H}} - v_{\mathrm{L}}}{L_1}t - i_{\mathrm{o}}. \end{cases} \tag{26}$$

Mode 2 [$t_1 < t < t_2$]: As shown in Fig. 5 (b), switch S_1 is turned off and the switch S_2 is turned on. During this mode, V_{L} charges L_1, L_2 and C_{b} while releasing energy to the load. So, i_{L_1}, i_{L_2} and $i_{C_{\mathrm{b}}}$ start to increase. The main equations relating the components during this time interval can be deduced as,

$$\begin{cases} i_{L_1}(t) = I_{L1V} + \dfrac{v_{\mathrm{H}} - v_{\mathrm{L}} - v_{\mathrm{Cb}}}{L_1}t, \\ i_{L_2}(t) = I_{L2V} + \dfrac{v_{\mathrm{L}}}{L_2}t, \\ i_{C_{\mathrm{b}}}(t) = -(I_{L1V} + \dfrac{v_{\mathrm{H}} - v_{\mathrm{L}}}{L_1}t), \\ i_{C_{\mathrm{H}}}(t) = I_{L1V} + \dfrac{v_{\mathrm{H}} - v_{\mathrm{L}}}{L_1}t - i_{\mathrm{o}}. \end{cases} \tag{27}$$

Based on the mode analysis and applying volt-second balance principle to inductors L_1 and L_2, voltage relationships in steady state among the input voltage, output voltage, and

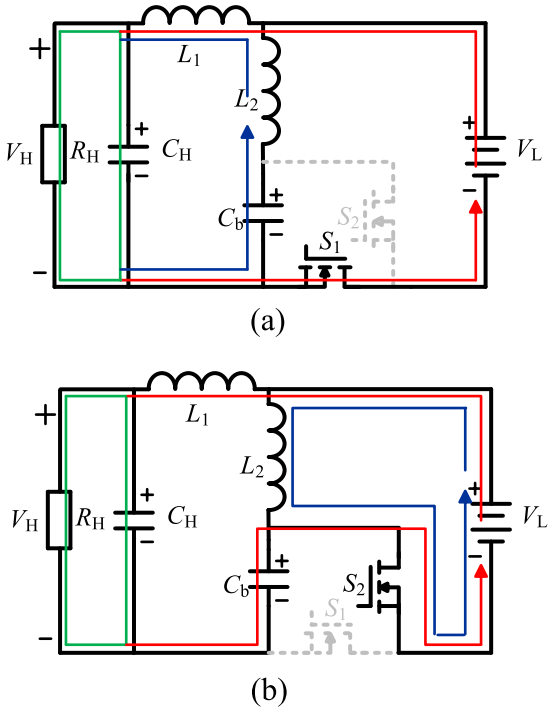

FIGURE 5. Equivalent circuits in step-up mode: (a) mode 1; (b) mode 2.

capacitor voltages can be obtained as,

$$\begin{cases}(V_{\rm L}-V_{\rm H})D+(V_{\rm L}+V_{\rm Cb}-V_{\rm H})(1-D)=0,\\(V_{\rm Cb}-V_{\rm L})D-V_{\rm L}(1-D)=0.\end{cases}\tag{28}$$

From (28), the voltage of capacitor $C_{\rm b}$ and the voltage of capacitor $C_{\rm L}$, i.e., the output voltage, can be derived as,

$$\begin{cases}V_{\rm Cb}=V_{\rm H},\\V_{\rm L}=DV_{\rm H}.\end{cases}\tag{29}$$

According to (29), the voltage conversion ratio of the proposed converter can be expressed as,

$$G_{step-up}=\frac{V_{\rm H}}{V_{\rm L}}=\frac{1}{D}.\tag{30}$$

2) CURRENTS OF INDUCTORS

Combining (26), (27), (29) and (6), the maximum and minimum values of the inductor currents can be calculated as,

$$I_{L1P}=I_{\rm o}+\frac{V_{\rm H}-V_{\rm L}}{2L_1}(1-D)T_{\rm s},\tag{31}$$

$$I_{L1V}=I_{\rm o}-\frac{V_{\rm H}-V_{\rm L}}{2L_1}(1-D)T_{\rm s},\tag{32}$$

$$I_{L2P}=\frac{1-D}{D}I_{\rm o}+\frac{V_{\rm H}-V_{\rm L}}{2L_2}(1-D)T_{\rm s},\tag{33}$$

$$I_{L2V}=\frac{1-D}{D}I_{\rm o}-\frac{V_{\rm H}-V_{\rm L}}{2L_2}(1-D)T_{\rm s}.\tag{34}$$

Then, average currents of L_1 and L_2 can be derived as

$$\bar{I}_{L1}=I_{\rm o},\tag{35}$$

$$\bar{I}_{L2}=\frac{1-D}{D}I_{\rm o}.\tag{36}$$

3) VOLTAGE AND CURRENT STRESSES OF POWER DEVICES

Based on the previous discussions, voltage stresses of the switches V_{S_1} and V_{S_2} are equal to the voltage of the capacitor $C_{\rm b}$ i.e., V_{Cb}, which is shown in (29).

According to Fig. 4(a), the peak value of the currents flowing through switches S_1 and S_2 can be derived as,

$$I_{\rm peak}^{S_1}=I_{L1P}+I_{L2P},\tag{37}$$

$$I_{\rm peak}^{S_2}=I_{L1P}+I_{L2P}.\tag{38}$$

By applying (30), (31), (33) to (37) and (38), we can have

$$I_{\rm peak}^{S_1}=I_{\rm peak}^{S_2}=\frac{1}{D}I_{\rm o}+\frac{(V_{\rm H}-V_{\rm L})^2}{2L_{\rm e}f_{\rm s}V_{\rm H}},\tag{39}$$

where $L_e=L_1//L_2$.

4) CALCULATION OF CRITICAL INDUCTANCE L_{1c} AND L_{2c}

When $I_{L1V}=0$, critical inductance of inductor L_1 can be derived as,

$$L_{1c}=\frac{(V_{\rm H}-V_{\rm L})(1-D)T_{\rm s}}{2I_{\rm o}}=\frac{R_{\rm H}(V_{\rm H}-V_{\rm L})^2}{2V_{\rm H}^2f_{\rm s}}.\tag{40}$$

Similarly, critical inductance of inductor L_2 can be derived as,

$$L_{2c}=\frac{R_{\rm H}V_{\rm L}(V_{\rm H}-V_{\rm L})}{2V_{\rm H}^2f_{\rm s}}.\tag{41}$$

When L_1 and L_2 are equal to their critical values, the converter operates in the BCM mode. Fig. 4 (b) shows some typical waveforms in BCM operation.

5) OUTPUT VOLTAGE RIPPLE ANALYSIS IN CCM

According to (21), voltage ripples of C_H can be calculated as,

$$v_{\rm CH-rip}^{CCM}=\frac{1}{C_{\rm H}}\int_{t_{01}}^{t_{02}}i_{C_{\rm H}}(t)dt=\frac{(V_{\rm H}-V_{\rm L})^3}{8L_1C_{\rm H}V_{\rm H}^2f_{\rm s}^2},\tag{42}$$

C. COMPARION OF THE PROPOSED NPIC CONVERTER AND OTHER BI-DIRECTIONAL DC-DC CONVERTERS

Comparisons between the NPIC converter proposed in this paper and other commonly used and previously proposed bidirectional converters are shown in TABLE 1. Compared with these converters, the proposed NPIC converter has the advantages of continuous input current in the step-down mode, simple structure with the fewest number of additional electronic devices.

III. SIMULATION VERIFICATION

In order to verify the effectiveness of the proposed converter, the converter topology is simulated in PSIM software environment with useful parameters shown in TABLE 2.

Step-down simulation results are demonstrated in Fig. 6 (a) and (b), which comprise the driving signals (v_{gs1} and v_{gs2}), input current ($i_{\rm in}$), output voltage ($v_{\rm o}$), inductor and switch currents (i_{L1}, i_{L2}, i_{S1} and i_{S2}), switch voltage stresses (v_{ds1} and v_{ds2}), respectively. Since inductor L_1 is in series with the power source, current of L_1 is equal to the input current,

TABLE 1. Performance comparison of various bi-directional dc-dc converters.

Converter types	Topologies	Input current in step-down mode	Voltage Stress of switch	Step-down gain	Step-up gain
Buck/boost	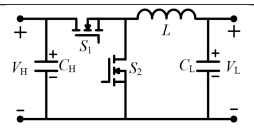	Intermittent	$V_{S_1} = V_{\mathrm{H}}$ $V_{S_2} = V_{\mathrm{H}}$	D	$\frac{1}{1-D}$
[16]	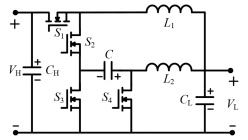	Intermittent	$V_{S_1} = \sqrt{V_{\mathrm{H}}V_{\mathrm{L}}} + V_{\mathrm{H}}$ $V_{S_2} = V_{\mathrm{H}}$ $V_{S_3} = \sqrt{V_{\mathrm{H}}V_{\mathrm{L}}}$ $V_{S_4} = \sqrt{V_{\mathrm{H}}V_{\mathrm{L}}}$	D^2	$\frac{1}{(1-D)^2}$
[17]	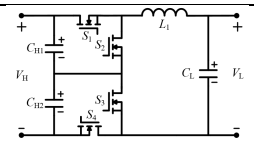	Intermittent	$V_{S_1} = V_{\mathrm{H}}/2$ $V_{S_2} = V_{\mathrm{H}}/2$ $V_{S_3} = V_{\mathrm{H}}/2$ $V_{S_4} = V_{\mathrm{H}}/2$	$\frac{D}{2}$	$\frac{2}{1-D}$
[18]	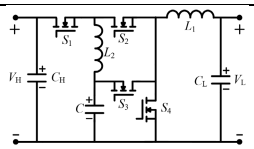	Intermittent	$V_{S_1} = V_{\mathrm{H}}$ $V_{S_2} = V_{\mathrm{H}}(1-D)$ $V_{S_3} = V_{\mathrm{H}}D$ $V_{S_4} = V_{\mathrm{H}}D$	D^2	$\frac{1}{(1-D)^2}$
Proposed NPIC converter	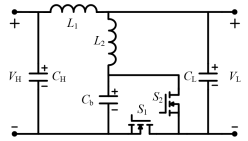	Continuous	$V_{S_1} = V_{\mathrm{H}}$ $V_{S_2} = V_{\mathrm{H}}$	D	$\frac{1}{D}$

TABLE 2. Simulation parameters.

Components	Parameter	
	Step-down	Step-up
Switching frequency (f_{s})	50kHz	50kHz
Duty cycle (D)	0.5	0.5
Input Voltage ($V_{\mathrm{H}}/V_{\mathrm{L}}$)	30V	15V
Load (R)	20Ω/10Ω	80Ω/30Ω
Inductors (L_1 and L_2)	200μH	200μH
Output capacitor ($C_{\mathrm{L}}/C_{\mathrm{H}}$)	200μF	200μF
Resonant capacitor (C_{b})	10μF	10μF

i.e., $i_{L1} = i_{\mathrm{in}}$. Fig. 7 shows the input current waveform of the proposed NPIC converter and the conventional buck/boost converter with the same simulation parameters. Apparently the proposed NPIC converter is able to regulate and draw non-pulsating input current into the converter system, demonstrating its superiority its conventional counterparts.

The step-up simulation results are demonstrated in Fig. 6 (c) and (d), which comprise the driving signals (v_{gs1} and v_{gs2}), input current (i_{in}), output voltage (v_{o}), inductor and switch currents (i_{L1}, i_{L2}, i_{S1} and i_{S2}), switch voltage stresses (v_{ds1} and v_{ds2}), respectively. According to Fig. 6 (c) and (d), this NPIC converter can obtain the same voltage gain as buck/boost bidirectional converter when working in the step-up mode.

IV. EXPERIMENTAL VERIFICATION

To further validate the effectiveness of the proposed converter, a prototype of the converter is built in this study,

TABLE 3. Experimental platform.

Equipment	Type
DC Power Supply	KIKUSUI PWR800L
Oscilloscope	KEYSIGHT DSO9104A
Current Probe	KEYSIGHT 1147A
Differential Probe	Agilent N2790A
Electronic Load	KIKUSUI TLZ334WH

TABLE 4. Experimental parameters.

Components	Parameter	
	Step-down	Step-up
Switching frequency (f_{s})	50kHz	50kHz
Duty cycle (D)	0.5	0.5
Input Voltage ($V_{\mathrm{H}}/V_{\mathrm{L}}$)	30V	15V
Load (R)	20Ω/10Ω	80Ω/30Ω
Inductors (L_1 and L_2)	200μH	200μH
Output capacitor (C_{L} / C_{H})	200μF/50V	200μF/100V
Capacitor (C_{b})	10μF/100V	10μF/100V
MOSFET (S_1, S_2)	IRF3205	IRF3205
Driving IC	TPL250	TPL250

with the physical prototype and experimental environment shown in Fig. 8 and TABLE 3, and the parameters used in the experiment are shown in TABLE 4.

A. STEP-DOWN MODE

Experimental results are demonstrated in Figs. 9∼11, which consist of the driving signals (v_{gs1}), output voltages (v_{L}), inductor currents (i_{L1} and i_{L2}), switch currents (i_{S1} and i_{S2})

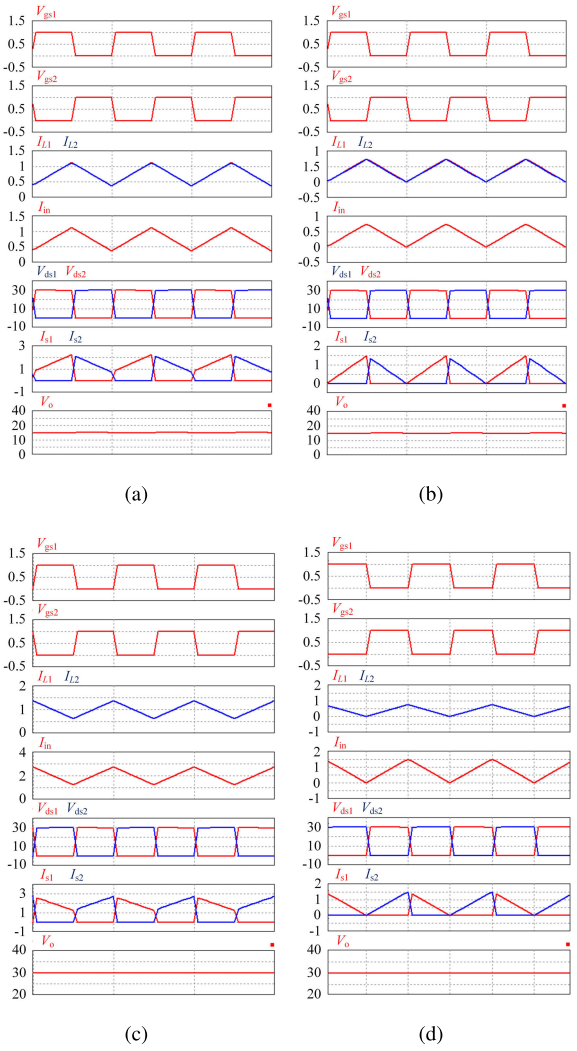

FIGURE 6. Simulation results for the proposed NIPC converter: (a) CCM in step-down mode; (b) BCM in step-down mode; (c) CCM in step-up mode; (d) BCM in step-up mode.

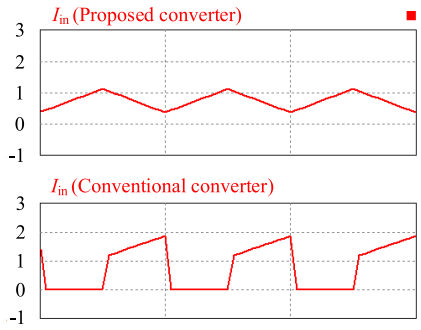

FIGURE 7. Input current of the proposed NPIC converter and conventional buck/boost converter in step-down mode.

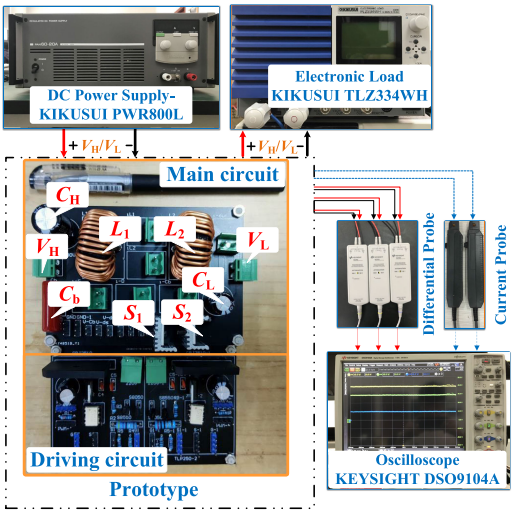

FIGURE 8. Prototype with the experimental environment.

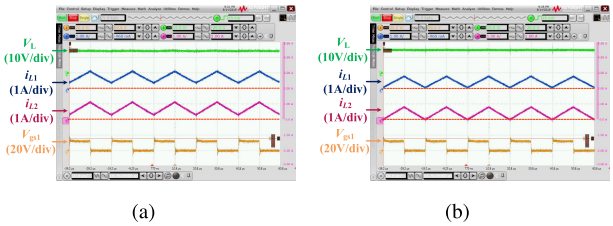

FIGURE 9. Experimental waveforms of the driving signal, output voltage, and the currents of inductors L_1, L_2 in step-down mode: (a) CCM; (b) BCM.

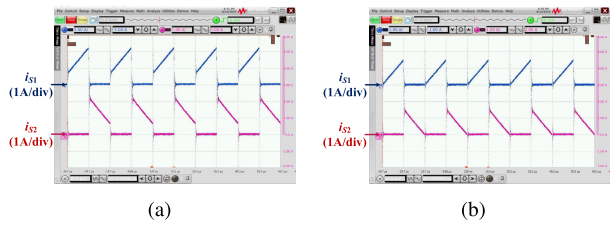

FIGURE 10. Experimental waveforms of the currents of switches S_1 and S_2 in step-down mode: (a) CCM; (b) BCM.

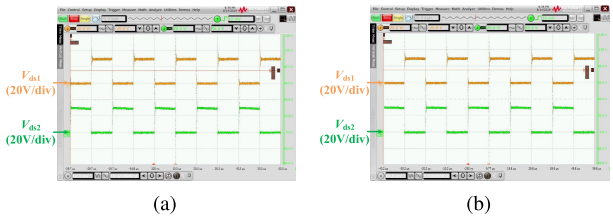

FIGURE 11. Experimental waveforms of the voltage stresses of the switch S_1 and S_2 in step-down mode: (a) CCM; (b) BCM.

and switch voltage stresses (v_{ds1} and v_{ds2}), respectively. As can be seen from Fig. 9, input currents ($i_{\text{in}} = i_{L_1}$) of the converter under both CCM and BCM modes are greater than 0. Obviously, the proposed converter can maintain a continuous and non-pulsating input current for the converter system. It is thus safe to state that the experimental results agree well with the theoretical analyses and stimulation

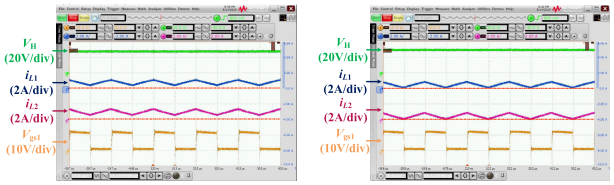

FIGURE 12. Experimental waveforms of the driving signal, output voltage, and currents of the inductors L_1, L_2 in step-up mode: (a) CCM; (b) BCM.

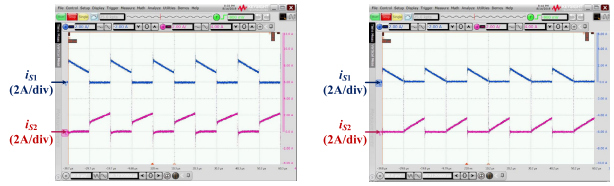

FIGURE 13. Experimental waveforms of the currents of switches S_1 and S_2 in step-up mode: (a) CCM; (b) BCM.

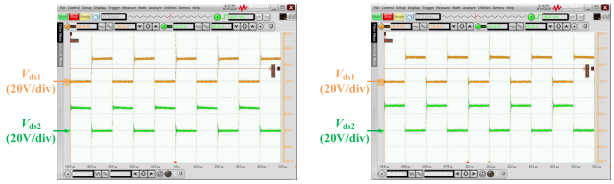

FIGURE 14. Experimental waveforms of the voltage stresses of the switch S_1 and S_2 in step-up mode: (a) CCM; (b) BCM.

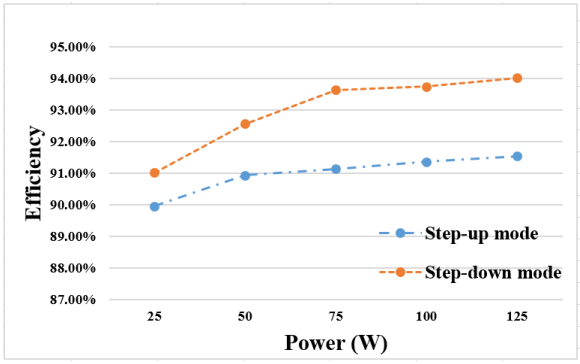

FIGURE 15. Efficiency of proposed converter with different operation power.

results, further proving the non-pulsating input current feature of the proposed NPIC converter.

B. STEP-UP MODE

In the step-up mode, experimental results are demonstrated in Figs. 12∼14, including driving signals (v_{gs1}), output voltages (v_H), inductor currents (i_{L1} and i_{L2}), switch currents (i_{S1} and i_{S2}) and switch voltage stresses (v_{ds1} and v_{ds2}), respectively. It can be seen from Figs. 12∼14 that the converter can achieve a stable output voltage. It can be concluded through experimentation that the proposed NPIC converter is able to retain the desired voltage gain in the step-up mode while producing non-pulsating input current in the step-down mode.

Fig. 15 shows efficiency curves of the proposed converter under different operation modes and power output, which demonstrates that the proposed converter has high efficiency. when the output power varies from 25 W to 125 W, the efficiency of the proposed converters is over 90%.

V. CONCLUSION

In this study, a novel bidirectional dc-dc converter converter with no inherent pulsating input current in step-down mode has been proposed. The proposed converter has lesser number of active and passive components. And in the step-down mode, the input current of the proposed converter in both CCM mode and BCM mode is greater than 0. In the step-up mode can retain the desired voltage gain. With the increase of the output power, the efficiency of the proposed converter promotes gradually. As it can be seen that the analysed efficiency is about 90-91.5% in the step-up mode and 91-94% in the step-down mode. This converter is a good candidate for applications like battery storage systems, which require continuous input current. Compared to traditional boost/buck bidirectional converters whose input current is inherently intermittent or pulsating, the proposed NPIC converter is able to produce a continuous non-pulsating input current in the step-down mode, overcomes the limitations of conventional converters and can better reserve the lifetime of electrochemically functioned dc sources such as batteries and fuel cells. The operating principle and steady-state performance of the proposed NPIC current have been first demonstrated in detail, which have then been corroborated through both simulation and experimentation, verifying the functionality and unique features of the proposed NPIC converter topology. It has also been proven in this study that the proposed converter has low output voltage ripples, high efficiency and the ability to remain the desired voltage gain in the step-up mode.

REFERENCES

[1] G. Zhang, Z. Li, B. Zhang, and W. A. Halang, "Power electronics converters: Past, present and future," *Renew. Sustain. Energy Rev.*, vol. 81, pp. 2028–2044, Jan. 2018.

[2] F. Xue, R. Yu, and A. Q. Huang, "A 98.3% efficient GaN isolated bidirectional DC–DC converter for DC microgrid energy storage system applications," *IEEE Trans. Ind. Electron.*, vol. 64, no. 11, pp. 9094–9103, Nov. 2017.

[3] D. Ma, W. Chen, L. Shu, X. Qu, X. Zhan, and Z. Liu, "A multiport power electronic transformer based on modular multilevel converter and mixed-frequency modulation," *IEEE Trans. Circuits Syst. II, Exp. Briefs*, vol. 67, no. 7, pp. 1284–1288, Jul. 2020, doi: 10.1109/TCSII.2019.2931529.

[4] G. Zhang, J. Yuan, Z. Li, S. S. Yu, S.-Z. Chen, H. Trinh, and Y. Zhang, "Forming a reliable hybrid microgrid using electric spring coupled with non-sensitive loads and ESS," *IEEE Trans. Smart Grid*, vol. 11, no. 4, pp. 2867–2879, Jul. 2020.

[5] A. Tong, L. Hang, G. Li, X. Jiang, and S. Gao, "Modeling and analysis of a dual-active-bridge-isolated bidirectional DC/DC converter to minimize RMS current with whole operating range," *IEEE Trans. Power Electron.*, vol. 33, no. 6, pp. 5302–5316, Jun. 2018.

[6] F. Zhang and Y. Yan, "Novel forward–flyback hybrid bidirectional DC–DC converter," *IEEE Trans. Ind. Electron.*, vol. 56, no. 5, pp. 1578–1584, May 2009.

[7] A. K. Rathore and U. Prasanna, "Analysis, design, and experimental results of novel snubberless bidirectional naturally clamped ZCS/ZVS current-fed half-bridge DC/DC converter for fuel cell vehicles," *IEEE Trans. Ind. Electron.*, vol. 60, no. 10, pp. 4482–4491, Oct. 2013.
[8] G. Chen, Y. Deng, L. Chen, Y. Hu, L. Jiang, X. He, and Y. Wang, "A family of zero-voltage-switching magnetic coupling nonisolated bidirectional DC–DC converters," *IEEE Trans. Ind. Electron.*, vol. 64, no. 8, pp. 6223–6233, Aug. 2017.
[9] L. Zhao, J. Chen, T. Chen, Y. Shi, Z. Fan, and Z. Zhuang, "Zero-voltage and zero-current-switching dual-transformer-based full-bridge converter with current doubler rectifier," *IEEE Trans. Power Electron.*, early access, May 25, 2020, doi: 10.1109/TPEL.2020.2997017.
[10] J. Huang, Y. Wang, Z. Li, and W. Lei, "Unified triple-phase-shift control to minimize current stress and achieve full soft-switching of isolated bidirectional DC–DC converter," *IEEE Trans. Ind. Electron.*, vol. 63, no. 7, pp. 4169–4179, Jul. 2016.
[11] X. Huang, F. C. Lee, Q. Li, and W. Du, "High-frequency high-efficiency GaN-based interleaved CRM bidirectional buck/boost converter with inverse coupled inductor," *IEEE Trans. Power Electron.*, vol. 31, no. 6, pp. 4343–4352, Jun. 2016.
[12] D. Baolei, L. Tao, H. Jun, J. Yang, and W. Xiao, "High-efficiency buck–boost converter and its control strategy suitable for wide voltage range," *J. Eng.*, vol. 2019, no. 10, pp. 7293–7297, Oct. 2019.
[13] I.-D. Kim, S.-H. Paeng, J.-W. Ahn, E.-C. Nho, and J.-S. Ko, "New bidirectional ZVS PWM sepic/zeta DC-DC converter," in *Proc. IEEE ISIE*, Jun. 2007, pp. 555–560.
[14] B. Zhu, F. Ding, and D. M. Vilathgamuwa, "Coat circuits for DC–DC converters to improve voltage conversion ratio," *IEEE Trans. Power Electron.*, vol. 35, no. 4, pp. 3679–3687, Apr. 2020, doi: 10.1109/TPEL.2019.2934726.
[15] E. Babaei and M. E. Seyed Mahmoodieh, "Analysis and investigation of energy transmission process in different operating modes of Sepic converter," *IET Power Electron.*, vol. 7, no. 4, pp. 819–828, Apr. 2014.
[16] H. Ardi, A. Ajami, F. Kardan, and S. N. Avilagh, "Analysis and implementation of a nonisolated bidirectional DC–DC converter with high voltage gain," *IEEE Trans. Ind. Electron.*, vol. 63, no. 8, pp. 4878–4888, Aug. 2016.
[17] C.-C. Lin, L.-S. Yang, and G. Wu, "Study of a non-isolated bidirectional DC–DC converter," *IET Power Electron.*, vol. 6, no. 1, pp. 30–37, 2013.
[18] H. Ardi, R. R. Ahrabi, and S. N. Ravadanegh, "Non-isolated bidirectional DC–DC converter analysis and implementation," *IET Power Electron.*, vol. 7, no. 12, 2014, pp. 3033–3044.
[19] G. Zhang, J. Yuan, S. S. Yu, N. Zhang, Y. Wang, and Y. Zhang, "Advanced four-mode-modulation-based four-switch non-inverting buck–boost converter with extra operation zone," *IET Power Electron.*, vol. 13, no. 10, pp. 2049–2059, Aug. 2020.
[20] M.-C. Cheng, C.-T. Pan, J.-H. Teng, and S.-W. Luan, "An input current ripple-free flyback-type converter with passive pulsating ripple canceling circuit," *IEEE Trans. Ind. Appl.*, vol. 53, no. 2, pp. 1210–1218, Mar. 2017.
[21] G. Zhang, S. Zou, S. S. Yu, S.-Z. Chen, B. Zhang, D. Qiu, and Y. Zhang, "Enhanced one-cycle control for multicell power converters," *IEEE Trans. Power Electron.*, vol. 35, no. 8, pp. 8846–8856, Aug. 2020.
[22] X. Liu and H. Li, "An electrolytic-capacitor-free single-phase high-power fuel cell converter with direct double-frequency ripple current control," *IEEE Trans. Ind. Appl.*, vol. 51, no. 1, pp. 297–308, Jan. 2015.
[23] Y. Ohnuma, K. Orikawa, and J.-I. Itoh, "A single-phase current-source PV inverter with power decoupling capability using an active buffer," *IEEE Trans. Ind. Appl.*, vol. 51, no. 1, pp. 531–538, Jan. 2015.
[24] W.-T. Fan, K. K.-F. Yuen, and H. S.-H. Chung, "Power semiconductor filter: Use of series-pass device in switching converters for filtering input current harmonics," *IEEE Trans. Power Electron.*, vol. 31, no. 3, pp. 2053–2068, Mar. 2016.
[25] V. Beldjajev, T. Lehtla, and J. Zakis, "Impact of component losses on the efficiency of the LC-filter based dual active bridge for the isolation stage of power electronic transformer," in *Proc. 8th Int. Conf.-Workshop Compat. Power Electron.*, Jun. 2013, pp. 132–137.
[26] O. Garcia, P. Zumel, A. de Castro, and A. Cobos, "Automotive DC-DC bidirectional converter made with many interleaved buck stages," *IEEE Trans. Power Electron.*, vol. 21, no. 3, pp. 578–586, May 2006.
[27] M. Ilic and D. Maksimovic, "Interleaved zero-current-transition buck converter," *IEEE Trans. Ind. Appl.*, vol. 43, no. 6, pp. 1619–1627, Nov./Dec. 2007.

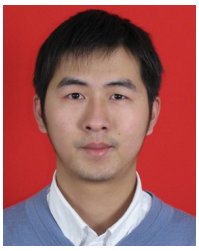

GUIDONG ZHANG (Member, IEEE) was born in Guangdong, China, in 1986. He received the B.Sc. degree from the Xi'an University of Technology, in 2008, and the two Ph.D. degrees from the South China University of Technology and FernUniversität, Hagen, in 2014 and 2015, respectively.

He is currently an Associate Professor with the School of Automation, Guangdong University of Technology, Guangzhou. His research interest includes power electronics topology and their applications.

NA JIN was born in Zhanjiang, Guangdong, China, in 1996. She received the B.Sc. degree from the Guangdong Normal University of Technology, Guangzhou, China, in 2019. She is currently pursuing the M.Sc. degree in electrical engineering with the School of Automation, Guangdong University of Technology, Guangzhou.

Her current research interest includes power electronics topology and their applications.

LILI QU was born in Hubei, China, in 1968. She received the B.S. degree in high-voltage technology and equipment from the Huazhong University of Science and Technology, Wuhan, Hubei, in 1989, the M.S. degree in control science and engineering from Xi'an Jiaotong University, Xi'an, Shanxi, China, in 2002, and the Ph.D. degree in power electronics from the South China University of Technology, Guangzhou, Guangdong, China, in 2009.

She is currently a Professor at Foshan University, China. Her research interests include power electronic systems and devices, switching power supply, and circuit analysis technology and its applications.

SAMSON SHENGLONG YU (Member, IEEE) received the master's degree (Hons.) in electrical and electronic engineering and the Ph.D. degree in electrical power engineering from The University of Western Australia (UWA), Perth, WA, Australia, in 2014 and 2017, respectively.

From 2017 to 2019, he served as a Postdoctoral Research Fellow at UWA. He is currently an Assistant Professor at Deakin University, Melbourne, VIC, Australia. His research interests include power system analysis, renewable energy integration and forecasting, and power electronics and its applications and control. He received the first and second Best Paper Awards in the IEEE Australia Paper Competition, in 2016 and 2017, the Best Reviewer Award for the IEEE TRANSACTIONS ON SMART GRID, in 2018, and the Featured Article in *Chaos: An Interdisciplinary Journal for Nonlinear Science*, in 2019.